Journal of
Biomedical Optics

BiomedicalOptics.SPIEDigitalLibrary.org

Toward jet injection by continuous-wave laser cavitation

Carla Berrospe-Rodriguez
Claas Willem Visser
Stefan Schlautmann
David Fernandez Rivas
Ruben Ramos-Garcia

SPIE.

Carla Berrospe-Rodriguez, Claas Willem Visser, Stefan Schlautmann, David Fernandez Rivas, Ruben Ramos-Garcia, "Toward jet injection by continuous-wave laser cavitation," *J. Biomed. Opt.* **22**(10), 105003 (2017), doi: 10.1117/1.JBO.22.10.105003.

Journal of Biomedical Optics 22(10), 105003 (October 2017)

Toward jet injection by continuous-wave laser cavitation

Carla Berrospe-Rodriguez,[a,*] Claas Willem Visser,[b,c] Stefan Schlautmann,[d] David Fernandez Rivas,[d] and Ruben Ramos-Garcia[a]
[a]Instituto Nacional de Astrofísica, Óptica y Electrónica, Departamento de Óptica, Puebla, Pue., México
[b]Harvard University, Wyss Institute for Biologically Inspired Engineering, Boston, Massachusetts, United States
[c]University of Twente, Physics of Fluids Group, MESA+ Institute and Faculty of Science and Technology, Enschede, The Netherlands
[d]University of Twente, Mesoscale Chemical Systems Group, MESA+ Institute and Faculty of Science and Technology, Enschede, The Netherlands

Abstract. This is a study motivated by the need to develop a needle-free device for eliminating major global healthcare problems caused by needles. The generation of liquid jets by means of a continuous-wave laser, focused into a light absorbing solution, was studied with the aim of developing a portable and affordable jet injector. We designed and fabricated glass microfluidic devices, which consist of a chamber where thermocavitation is created and a tapered channel. The growth of a vapor bubble displaces and expels the liquid through the channel as a fast traveling jet. Different parameters were varied with the purpose of increasing the jet velocity. The velocity increases with smaller channel diameters and taper ratios, whereas larger chambers significantly reduce the jet speed. It was found that the initial position of the liquid–air meniscus interface and its dynamics contribute to increased jet velocities. A maximum velocity of $94 \pm 3\ \mathrm{m/s}$ for a channel diameter of $D = 120\ \mu\mathrm{m}$, taper ratio $n = 0.25$, and chamber length $E = 200\ \mu\mathrm{m}$ was achieved. Finally, agarose gel-based skin phantoms were used to demonstrate the potential of our devices to penetrate the skin. The maximum penetration depth achieved was ∼1 mm, which is sufficient to penetrate the stratum corneum and for most medical applications. A meta-analysis shows that larger injection volumes will be required as a next step to medical relevance for laser-induced jet injection techniques in general. [DOI: 10.1117/1.JBO.22.10.105003]

Keywords: needle-free; jet; injection; continuous-wave laser; microfluidic; cavitation.

Paper 170446R received Jul. 10, 2017; accepted for publication Sep. 15, 2017; published online Oct. 13, 2017.

1 Introduction

Needles are a common and efficient method for drug delivery, used for more than two centuries. However, it presents serious health issues, such as waste contamination, risk of spreading diseases, unwanted needle-stick incidences, pain, and phobia, among others.[1] The reuse of needles is a common practice, which may transmit contagious diseases and deadly viruses. In Africa, it is estimated that 20 million injections contaminated with blood from HIV-infected patients are administered inadvertently every year.[2] In addition, according to the World Health Organization, unsafe injections in the year 2000 will lead to 9 million deaths between 2000 and 2030.[3]

Any candidate device to replace the widely used needles must be cheap, portable, easy to operate, and safe. Such a device should be reusable, no physical contact should take place between the device and the skin of the patient, reducing contamination risks. Different mechanisms for needle-free jet injection have been investigated.[4–21] These can be classified as impulsive pressure-induced jets, such as compressed gas, spring[6,7] or piezoelectric transducer,[8–10] and cavitation-induced jets, such as electric current[11] or laser.[17–21] Particularly, spring and compressed gas systems are now commercially available, which are mostly used for insulin injection.[13–16]

The potential of cavitation-induced jets by lasers was first explored by studying cavitation bubbles near to an elastic boundary.[22,23] Laser-based systems produce extremely fast jets (up to ∼850 m/s) and reach an injection depth of 5 mm,[24] which is sufficient for most medicines, and can operate without cross-contamination. In this case, pulsed lasers are used to generate plasma or vapor bubbles which, in turn, emit pressure waves of several GPa of amplitude.[25,26] The required pulsed lasers are expensive, noisy, and heavy. Recently, we demonstrated a jet injector, which is based on continuous-wave (CW) laser cavitation[27] (or thermocavitation[28–31]). These lasers are widely used and have the benefits of being lightweight, cheap, and pose a much lower safety risk than pulsed lasers for a given amount of light energy, as the irradiance is lower. However, the injection velocities were still limited to 30 m/s, which is barely sufficient to penetrate the outer skin layer (stratum corneum, which has a thickness of 10 to 40 μm),[32] and the injection depth was not assessed.

In this work, we present a microfluidic device that resolves this issue. A tapered shaped channel enhances the jet velocity in combination with dynamic focusing. Experiments of liquid jet penetration into agarose gel at 1% were also performed as a proof of concept for an eventual use of these designs in injection devices. CW lasers may solve the problem of integrability in portable devices since they are compact, cheap, and powerful enough to achieve jet speeds able to penetrate skin. Finally, we present an overview of different jet injection methods and discuss current applications of laser-based jet injection as

---

*Address all correspondence to: Carla Berrospe-Rodriguez, E-mail: cberrospe@inaoep.mx

well as future avenues toward the improvement of CW laser-based systems.

2 Materials and Methods

The setup depicted in Fig. 1(a) was used to study the bubble dynamics and the corresponding liquid jet propagation. Thermocavitation was produced by light absorption in a copper nitrate saturated solution. The laser ($\lambda = 790$ nm) was focused at the bottom of the device chamber with a 10× microscope objective. The spot produced an intensity of $I = 2.6 \times 10^4\ \mathrm{W/cm^2}$ ($P = 116$ mW and beam waist of $\sim 17\ \mu$m). The microfluidic device was placed on a XYZ linear translation stage holder in order to align it with respect to the laser spot. A fast camera (FASTCAM SA-X2) and a white-light source (Olympus LP-1) were placed at different locations to study two different events: (1) jet propagation (velocity and shape) and (2) liquid penetration into agarose gel, as indicated in Fig. 1(a). These events were recorded at 300,000 frames-per-second (fps) and 125,000 fps, respectively. The laser current was controlled with square wave signal from a function generator, which also triggered the fast camera. The laser was turned on for 500 ms, which allows to observe a full cycle of bubble expansion and collapse. If the laser current is not modulated, then a quasiperiodic bubble formation, whose frequency is controlled with the laser intensity, takes place.[30]

2.1 *Description of the Device*

Microfluidic chips were designed and fabricated in glass substrates under clean-room conditions. Two wafers of Boroflat glass were identically micromachined with wet-etching in hydrogen fluoride solutions, and then placed together with anodic bonding. The bonded wafers were then diced in chips with dimensions of $10 \times 8\mathrm{mm}^2$. The chips were constituted by (i) a channel inlet (400-μm depth); (ii) a circular container (100-μm depth); (iii) an s-shaped channel (100-μm depth), to provide fluid resistance and control over the liquid volume inside the device; (iv) a chamber (100-μm depth), where the cavitation bubble is created; and (v) a straight or tapered channel (100-μm depth) for liquid propagation and confinement, as is shown in Fig. 1(b).

The device geometrical parameters that affect the liquid jet velocity are the channel diameter at the exit D_x, channel diameter before the tapering d, taper ratio $n = \frac{D_x}{d}$, and chamber length E, as shown in Fig. 1(b). Several devices were fabricated with dimensions of $D_x = 120$, 200, 300, and 500 μm, $D_y = 100\ \mu$m, where D_y is two times the etched depth, and E ranges from 200 to 1000 μm. Although the cross-section of the channel was not axisymmetric, it has been demonstrated that for asymmetric nozzles, the jets spread only slightly faster at subsonic conditions (<340 m/s),[33] which is our case. Hence, the generated jets in this study can be assumed as cylindrical.

In previous reports, it was found that the cavitation bubble expansion rate is proportional to the chamber width.[27,34] For this reason, this parameter was set to 1000 μm, which is sufficiently large to allow a fast expansion, and on the other hand, not too large as to waste its kinetic energy in displacing a large liquid volume, which may slow down the jet speed.

The channel length was set at 500 μm, however, it extended beyond the outlet of the device, as shown in Fig. 1(b). This was done to prevent changes in the taper ratio values previously established, due to the lack of precision in the cutting and separation process of individual devices from the wafer. The liquid inlet was connected to a 1-mL plastic syringe Terumo (Terumo medical products) through a glass capillary tube with 360 μm diameter, using a microfluidic fitting and a connector. The

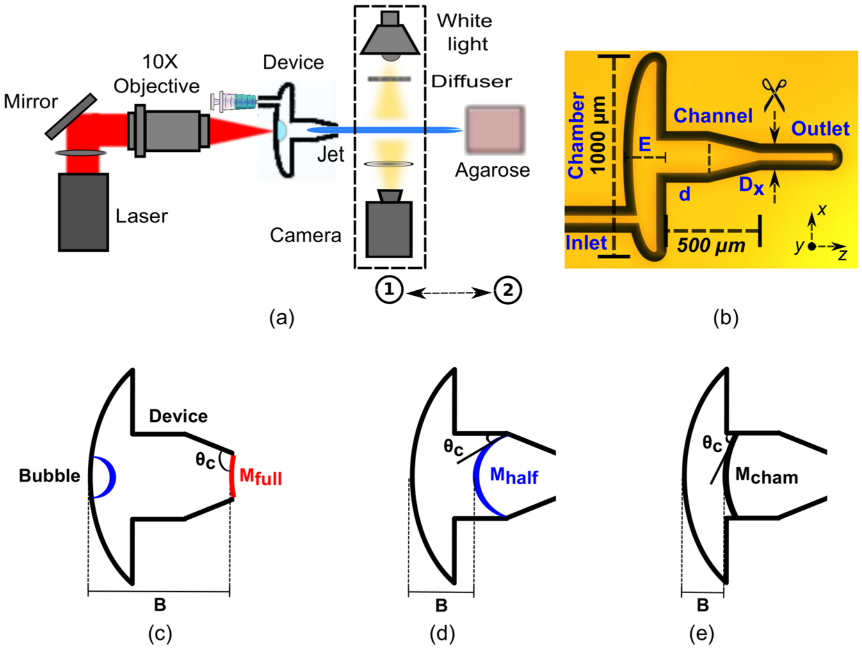

Fig. 1 (a) Setup for liquid propagation. The visualization setup is indicated by the dashed line, and could be moved from (1) to (2) to measure: (1) liquid expelled from the tapered channel and (2) penetration of the jet into agarose gel 1%. (b) Photograph of a microfluidic device with a tapered channel to increase its velocity ($D_x = 120\ \mu$m, $n = 0.5$, and $E = 200\ \mu$m). Image from a confocal microscope. (c) Meniscus M_{full} and the parameters B and θ_c. (d) Meniscus M_{half} and (e) Meniscus M_{cham}.

syringe was used to manually control the position of the meniscus in the channel by changing the liquid volume inside the cavity. A saturated solution of copper nitrate (13.78 g in 10 mL of water), with an optical absorption coefficient of 130 cm^{-1} for the laser wavelength, was used to produce the cavitation bubble.[29]

Agarose gel (Sigma-Aldrich) at 1% was prepared in small cubes of 4 mm^3 approximately, to characterize the penetration depth of the liquid jets produced by the devices. It has been proved that agarose gel is an appropriate model to compare with human skin,[35] since its mechanical properties are similar to soft tissue in the body.[36] However, it is important to mention that human skin, specially, the stratum corneum (outermost layer of skin) is a very complex tissue and its properties change significantly depending on the part of the body. The Young's modulus of skin can have values ranging from 20 kPa to 2 MPa, depending on the part of the body and per individual (age, hydration level, and many other characteristics).[32,37] The Young modulus and plastic yield stress of agarose at 1% are around 40[38] and 30 kPa,[39] respectively, which lies on the lower limit of the skin Young's modulus.

2.2 *Position of the Meniscus*

The presence of a concave liquid–air interface plays a crucial role on achieving high speed liquid jets.[17] In fact, the dynamic focusing, driven by the pressure wave produced by optical breaking, is due to the initial contact angle of the liquid with the channel walls. The meniscus concavity can be tuned using surfactants to reduce or increase the contact angle.[17,40,41] For large contact angles (~90 deg), the jet speed is minimum but increases as the contact angle is reduced. We confirm these findings, but, since the device configuration is different from capillary tubes used before,[17] we have investigated this effect further.

The parameters that characterize the liquid–air interface are shown in Fig. 1(c), the distance between the laser focus (where the bubble is created) and the meniscus position is B, whereas θ_c is the initial contact angle of the meniscus. The initial contact angle was obtained with the relation:[17]

$$\cos\,\theta_c = \frac{d}{2R_c}, \tag{1}$$

where R_c is the radius of curvature of the meniscus.

The initial radius of curvature is varied by minor adjustments of the liquid volume with the syringe. The three cases under study were M_{full} (i.e., the meniscus formed is rather small and the contact angle is ~90 deg), meniscus M_{half} (the device filled until half of the channel), and M_{cham} (only the chamber device is filled), as shown in Figs. 1(c)–1(e), respectively. The values of B and θ_c for each case in the device with parameters D_x 120 μm, $E = 200$ μm, and $n = 0.5$ are presented in Table 1.

Table 1 Values of the parameters describing the meniscus characteristics and the corresponding jet velocity for device with $D_x = 120$ μm, $n = 0.5$ and $E = 200$ μm.

Meniscus	B (μm)	θ_c
$\mathrm{M}_{\mathrm{full}}$	700	90
$\mathrm{M}_{\mathrm{half}}$	450	47
$\mathrm{M}_{\mathrm{cham}}$	200	68

3 Results

3.1 *Jet Velocity Parametric Study*

Figure 2 shows a typical example of the jets produced by the fast expanding bubble in a device with the following parameters: $D_x = 120$ μm, $n = 0.5$, $E = 200$ μm and laser intensity $I = 2.6 \times 10^4$ $\mathrm{W/cm^2}$, for the meniscus M_{full}, M_{half}, and M_{cham}. The bubble drives the meniscus dynamic through the channel, leading to dynamic focusing of the flow and finally to a jet. For M_{cham}, the jet has a tip around five times smaller than the rest of its body, with a speed up to 75 ± 3 m/s during the first 8 μs, while M_{half} and M_{full}, only 45 ± 4 m/s and 25 ± 1 m/s, respectively.

With these image sequences, we can observe that for M_{cham} ($B = 200$ μm), a sharp jet is formed. When B increases, the liquid jet becomes less focused and its sharpness decreases (M_{half}). Finally, when no meniscus is present (M_{full}, $B = 700$ μm), there is no focusing and therefore, the jet becomes blunt, due to the liquid adhesion to the walls of the output channel. Under these circumstances, the fluid is pushed outside of the device with a tip bigger than the rest of the jet.

The jet velocity V_{jet}, as a function of the taper ratio n, for a channel diameter $D = 120$ μm, chamber length $E = 200$ μm, and laser intensity of $I = 2.6 \times 10^4$ $\mathrm{W/cm^2}$, is shown in Fig. 3(a). As expected, the jet velocity increases as the taper ratio is reduced. However, the meniscus position and shape have a substantial effect on the jet velocity. For M_{half} and M_{cham}, ~60% increase on the velocity was achieved when n decreased from 1 to 0.25. For M_{full}, the jet velocity is practically independent of the taper ratio n. This result highlights the importance of dynamic focusing to achieve high speed jets. It is expected that flow through a tapered channel increases the velocity according to the principle of continuity as

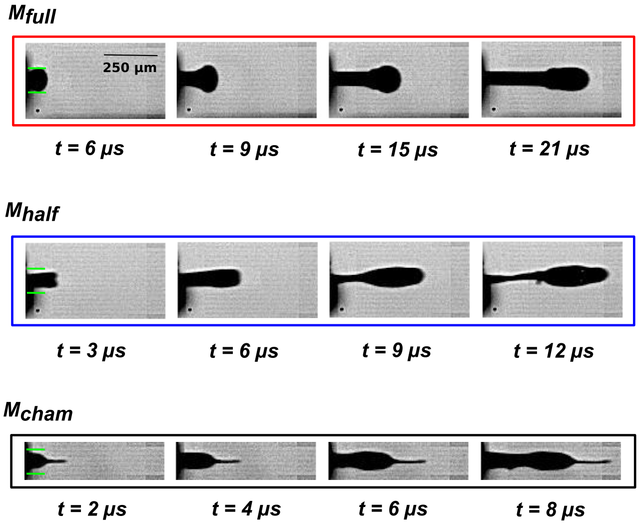

Fig. 2 Time series of the initial shape of the jet due to dynamic focusing for meniscus M_{full}, M_{half}, and M_{cham}. This follows from images recorded at 300,000 fps for M_{full} and M_{half}, and at 450,000 fps for M_{cham}. The green (online color) lines indicate the diameter of the channel device.

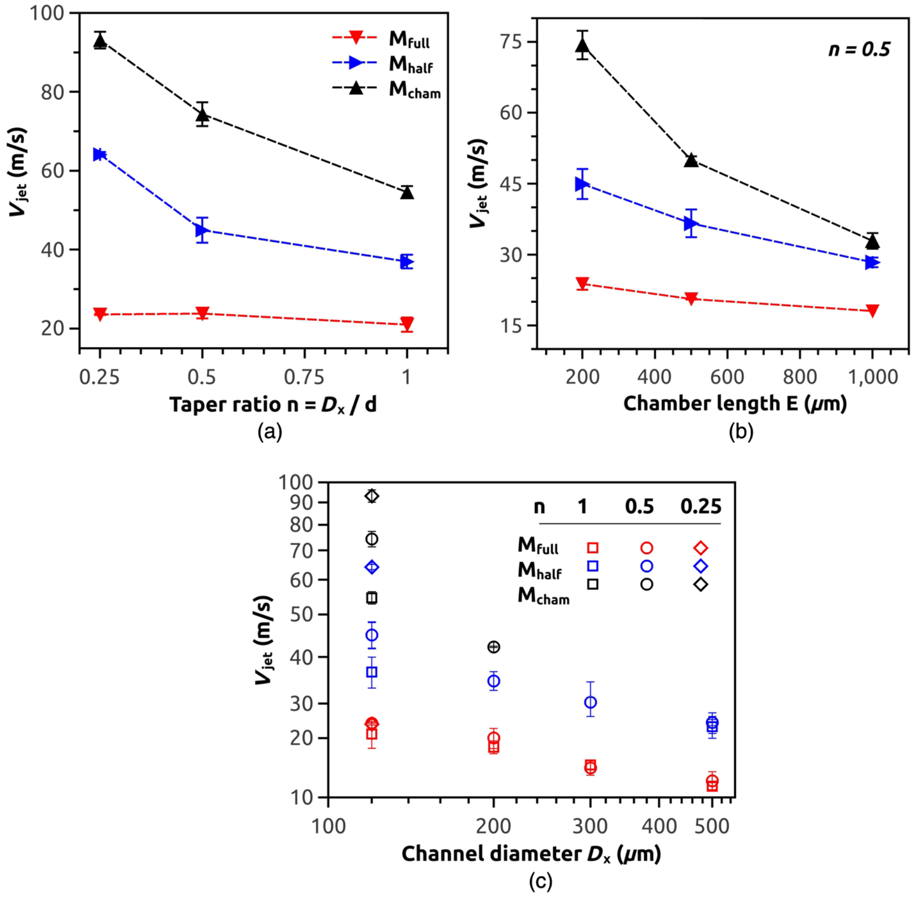

(a) (b) (c)

Fig. 3 Jet velocity with a laser intensity of $I = 26 \times 10^3\ \mathrm{W/cm^2}$ as a function of: (a) taper ratio n, for $D_x = 120\ \mu\mathrm{m}$ and $E = 200\ \mu\mathrm{m}$. (b) Chamber length E, for $D_x = 120\ \mu\mathrm{m}$ and $n = 0.5$ and (c) channel diameter D_x, for $E = 200\ \mu\mathrm{m}$ and different taper ratios n.

$V_{\mathrm{jet}} = \frac{1}{n^2} V_D$, where V_D is the velocity inside the channel with diameter D.[42] Thus, for taper ratio of 0.25, the jet velocity increases by a factor of 16. This finding is in disagreement with the mere 1.6 ratio observed in the experiments [see Fig. 3(a)]. The following reasons are attributed to this mismatch. The chamber is not filled completely, and the liquid is displaced by a half hemisphere shaped bubble and not by a constant plane as in the Bernoulli equation. Then, for the latest case, the exerted pressure is constant, whereas for our case, there is a pressure gradient. Since the channel is partially empty, friction may also play an important role reducing the jet velocity.

The dependence of the chamber length E on the jet velocity is shown in Fig. 3(b) for M_{full}, M_{half}, and M_{cham}. Note that the fastest jets were obtained for the smallest length ($B = 200\ \mu\mathrm{m}$) regardless of the initial contact angle value. These results are in good agreement with previous studies in capillary tubes, where it was found that the jet velocity is inversely proportional to B.[17] In addition, the focused jet is no longer in contact with the channel walls, hence, kinematic friction is reduced. These results confirm the relevance of dynamic focusing for M_{cham}. In capillary tubes, where the walls are parallel, a smaller contact angle results in faster jets. However, in tapered channels, it is not necessarily true. Larger contact angles, in combination with the device geometry, can lead to more efficient focusing, as is shown here.

The jet velocity as a function of channel diameter for different taper ratios n is shown in Fig. 3(c). The jet velocity increases as both the channel diameter and the taper ratio are reduced. However, for diameters $D \geq 300\ \mu\mathrm{m}$, the velocity remains almost independent of the taper ratio. As the diameter increases, the fluid confinement is reduced and the liquid is less focused, giving as a result the reduction of the jet speed to a minimum value. Based on the results shown, a maximum jet velocity up to $94 \pm 3\ \mathrm{m/s}$ was observed for the following parameters: $D_x = 120\ \mu\mathrm{m}$, $n = 0.25$, $E = 200\ \mu\mathrm{m}$, and M_{cham} ($B = 200\ \mu\mathrm{m}$ and $\theta_c = 68$ deg).

The initial conditions of the meniscus not only influence the jet velocity but its shape, too. A meniscus as near as possible to the bubble formation place and a small contact angle $\theta_c \leq 68$ deg are the conditions that will lead to a fast and sharp jet. As was observed before, in order to increase the jet velocity, the taper ratio, chamber length, and channel diameter need to be reduced. However, the reduction of these parameters will eventually lead to an early breakup of the jet into small droplets, changing from a jet regime to spray regime.[43]

3.2 *Skin Phantom Penetration*

The performance of the fabricated devices to generate jets was tested for skin phantom penetration. The penetration depth L into agarose 1% gel cubes as a function of channel diameter and jet velocity for meniscus M_{half} was measured. The velocities obtained for M_{full} ($V_{\mathrm{jet}} \sim 13$ to $25\ \mathrm{m/s}$) are not high enough to obtain a large penetration into agarose, whereas in the case of

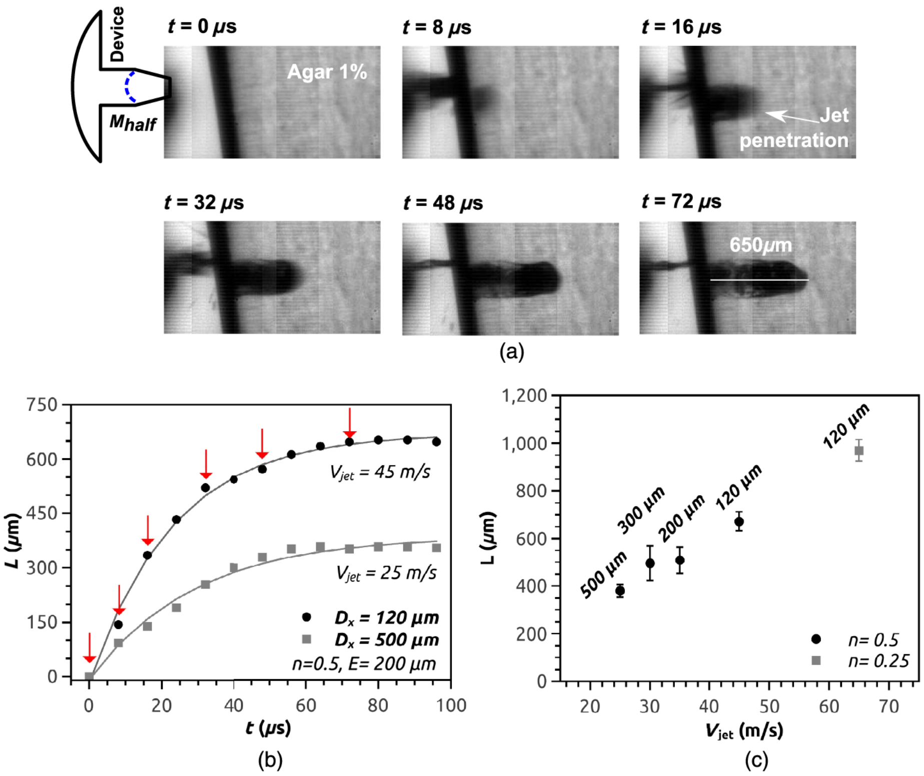

Fig. 4 (a) Image sequence of the liquid jet penetration into agarose 1% gel recorded at 125,000 fps for $D_x = 120$ μm, $n = 0.5$, $E = 200$ μm, and M_{half} (see Video 1, MOV, 376 KB [URL: http://dx.doi.org/10.1117/1.JBO.22.10.105003.1]; Video 2, MOV, 158 KB [URL: http://dx.doi.org/10.1117/1.JBO.22.10.105003.2]; Video 3, MOV, 378 KB [URL: http://dx.doi.org/10.1117/1.JBO.22.10.105003.3]). The penetration depth in this case was $L_{\max} = 650$ μm. (b) Penetration depth as a function of time for $n = 0.5$, $D_x = 120$ μm, and $D_x = 500$ μm, respectively. The red arrows indicate the moment where images from (a) were taken. An exponential growth curve was fitted into the data. For 45 ± 4 m/s jet, $L_{\max} = 675 \pm 11$ μm and $t_0 = 24 \pm 1$ μs, while for 25 ± 1 m/s jet, $L_{\max} = 390 \pm 13$ μm and $t_0 = 30 \pm 3$ μs. (c) Penetration depth as a function of liquid jet velocity. The channel diameter of each device for each velocity obtained is indicated at the top of the data points.

M_{cham} ($V_{\text{jet}} \sim 45$ to 94 m/s), the thickness of the jet tip is too small, so it was difficult to observe the real penetration depth in the gel with the fast camera. Thus, meniscus M_{half} was chosen since the jet velocities ($V_{\text{jet}} \sim 25$ to 65 m/s) are sufficiently high.

A jet expelled from the channel, and breaking through the gel with a velocity of 45 ± 4 m/s, is shown in the image sequence of Fig. 4(a). In this particular case, the jet penetrated a maximum distance of $L_{\max} = 650$ μm in $t = 96$ μs. The penetration depth L, as a function of time, is shown in Fig. 4(b). These values were calculated from image sequences, as presented in Fig. 4(a). A data fitting curve shows a behavior of the form $L(t) = L_{\max}(1 - e^{\frac{-t}{t_0}})$. The exponential behavior was predicted in Ref. 24.

The penetration depth as a function of the jet velocity for $n = 0.5$ and $n = 0.25$ is shown in Fig. 4(c). As expected, the penetration depth increases as the jet velocity increases. A maximum penetration depth up to ~1 mm was achieved for $D = 120$ μm and $n = 0.25$. The parameters studied in the microfluidic devices and how they affect the penetration depth of the liquid jet into agarose are shown in Table 2. It can be observed that by reducing the parameters of the device D_x, n, and E, and by reducing the liquid–air interface parameters B and θ_c, the penetration depth L will reach its maximum.

The liquid volume injected in the gel was calculated from the initial liquid volume contained inside the device, and subtracting the remaining liquid once the jet is expelled, assuming evaporation is minimal. For $D_x = 120$ μm, ~40 nL were introduced into the agarose, whereas for $D_x = 500$ μm, a volume of 157 nL was delivered.

4 Discussion

An overview of jet velocity measurements for both pulsed-laser and our CW laser system is provided in Table 3. In both laser configurations (pulsed and CW), a pressure wave is created by vaporizing a small amount of liquid. However, in thermocavitation (CW laser), the intensity threshold to produce bubble nucleation is several orders of magnitude smaller than for pulsed systems, as a sufficient amount of energy can be delivered over a longer time span. For example, a pulsed laser intensity around $I = 13 \times 10^{10}$ W/cm^2 was necessary to generate jets of 100 m/s in previous work,[17] whereas for our CW system, an energy of $I = 26 \times 10^3$ W/cm^2 was required.

Remarkably, for CW lasers, the jet velocity decreases with increasing laser intensities, in contrast to results for pulsed lasers.[17] This is due to the fact that the spinodal limit is achieved faster as the laser intensity is increased. Therefore, for high laser intensities, thermal confinement is achieved faster, limiting the bubble size, whereas for lower intensity, heat diffusion allows greater superheated volume and therefore bigger vapor bubbles.[27,29] Jets generated with CW lasers may therefore

Table 2 Penetration depths *L* dependence on the geometrical parameters of the microdevice, and parameters of the liquid–air interface. The up arrow and down arrow indicate an increment and a reduction on those parameters, respectively. The number of circles in *L*, represent the penetration length.

Channel diameter D_x (120 to 500 μm)	Taper ratio n (0.25 to 1)	Chamber length E (200 to 1000 μm)	Contact angle θ_c (47 deg to 90 deg)	Bubble distance B (200 to 700 μm)	Penetration L (0.390 to 1 mm)
⇑	⇑	⇑	⇑	⇑	●
⇓	⇑	⇑	⇑	⇑	●●
⇓	⇓	⇑	⇑	⇑	●●●
⇓	⇓	⇓	⇑	⇑	●●●●
⇓	⇓	⇓	⇓	⇑	●●●●●
⇓	⇓	⇓	⇓	⇓	●●●●●●

Table 3 Laser characteristics of recent investigations in jet injection systems and maximum jet velocity achieved.

Laser	τ_p (ns)	$E(\mathrm{mJ})/I(\mathrm{W/cm^2})$	$V_{\max}$ (m/s)	Ref.
Nd: YAG 1064 nm	5.5	1400/—	200	44
Nd:YAG 532 nm	5–9	100/—	264	20
Nd: YAG 532 nm	6	$0.15/12.7\times 10^{10}$	850	17
Er:YAG 2940 nm	2500	1000/—	45	18
Nd:YAG 532 nm	6	$20/17\times 10^{12}$	250	24
Nd: YAG 1064 nm- Er: YAG 2940 nm	7-2500	408/—	30–80	19
Infrared laser 790 nm	—	$—/26\times 10^{3}$	30	27
Infrared laser 790 nm	—	$—/26\times 10^{3}$	94	This work

have a lower maximal velocity compared to pulsed lasers, but the current work shows that these velocities are still sufficient for injection purposes.

Common injected drugs include antibiotics, steroids, hormones, vaccines, and insulin, among others. Typical dosage volume and injection depth of these medicines are plotted in Fig. 5(a). In addition, the volume injected, per injection event, as a function of penetration depth, for different jet injection methods, is shown in Fig. 5(b). It can be observed that for impulsive pressure-induced jet systems (spring, gas, chemical reaction, and piezoelectric actuator), the injected volume reaches medical doses like insulin, vaccines, and antibiotics. By contrast, for cavitation-induced systems (electric current, pulsed laser, and CW laser), the maximum volume achieved (1 μl) is still below the medical doses.

The liquid quantities injected by these laser systems are too small for typical drug doses still. Repeated injection may offer a solution to this problem, as cavitation repetition rate of 4 kHz could be reached,[29,30] so a typical dose of 1 ml could be achieved in a few seconds. Further investigations from a medical perspective would be required to validate this approach.[66] As shown in Fig. 5(a), applications where the volumes required are smaller, such as allergy tests,[67] medical tattooing,[57] and microdosing for clinical study[68–70] could be achieved with CW laser-based injection.

Another important issue to further investigate in our device is the injection of real drugs for medical treatment, instead of the copper nitrate solution we have used in this investigation. One option could be to use different laser wavelengths according to the absorption coefficient of the drug, however, this will probably affect the chemistry of the injected solution in an undesired way. In order to avoid this, it is necessary to thermally isolate the cavitating liquid from the drug one, as proposed elsewhere.[20] Additionally, the jetting of liquid drugs with different viscosities needs to be studied for possible implications in jet velocity and skin penetration depth, as was recently investigated with the use of impulsive pressure acceleration for the generation of highly viscous jets.[71]

The penetration depth $L_{\max}$ values presented in this work are comparable with previously reported results obtained for pulsed laser,[24] where a depth of 1 mm was reached for a jet speed of 50 m/s in a capillary tube with 500 μm of diameter. Earlier studies[22,23] have demonstrated jet velocities up to 960 m/s penetrating an elastic boundary, even through a water layer of 350 μm. Yet another investigation, where cavitation-induced jets were generated by an electric discharge, penetration depths up to 450 μm were achieved, with jet velocities between 130 and 270 m/s.[11] Notwithstanding the higher velocities than those we obtained here, less penetration depth was achieved. This may be attributed to the large scatter nature of the jets.

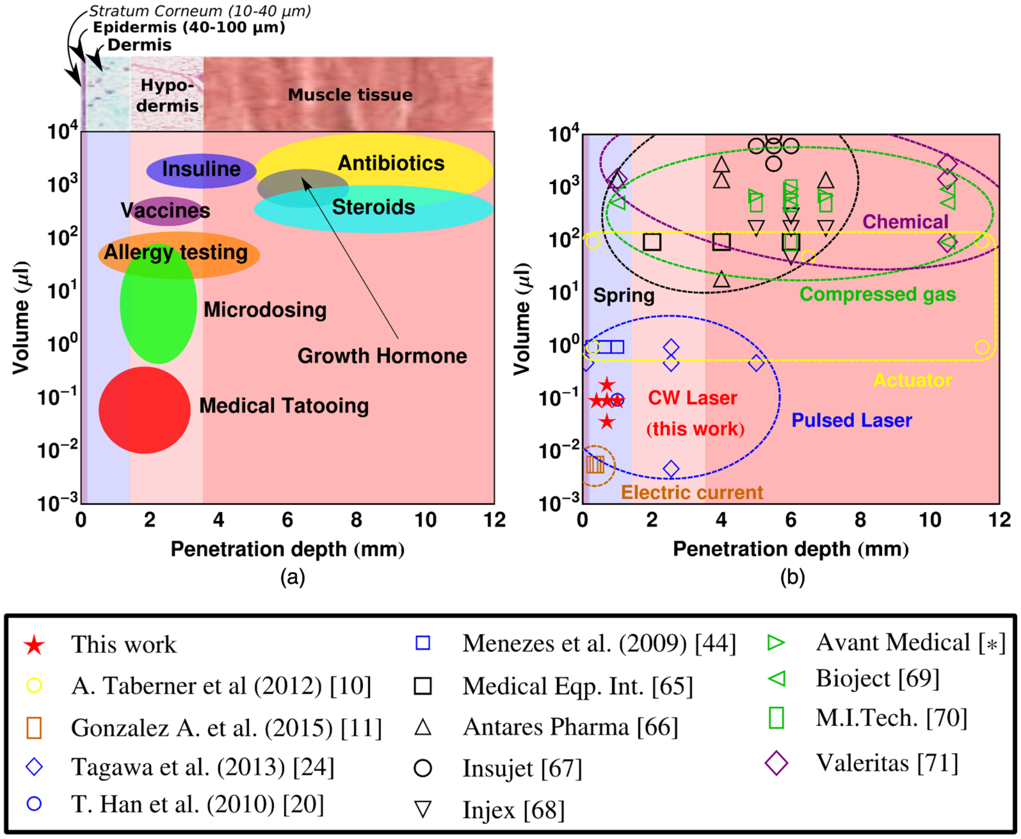

Fig. 5 (a) Typical volume and penetration depth of commonly used medicines: antibiotics,[45] growth hormone,[46] steroids,[47,48] insulin,[49,50] vaccines,[51–53] allergy testing,[54] microdosing[55,56] and medical tattooing.[57,58] At the top, cross section of the human skin layers from outermost (stratum corenum) to muscle. (b) Injected volume as a function of penetration depth for different jet injection systems (nonexhaustive research). The maximum, minimum and mean liquid volume achieved per injection event by each system are indicated by different markers, while the type of generation mechanism is represented by color (black: spring,[59–62] green: gas,[63,64] violet: chemical reaction,[65] blue: pulsed laser,[20,24,44] yellow: actuator,[10] orange: electric current[11] and red: CW laser, this work). At the bottom, the reference of each device plotted is shown.

According to the literature,[72] the stratum corneum has a thickness between 10 and 40 μm, whereas the epidermis is between 40 and 100 μm, depending on the part of the body. Therefore, by combining CW laser and microfluidics systems, it should be possible to penetrate human skin, opening, for the first time, the possibility of cost-effective, portable, and silent jet injection technologies for intra- or transdermal drug delivery.

5 Conclusion

CW laser-based cavitation is a mechanism to produce jets with sharp shapes and velocities sufficiently high to penetrate the skin. Here, different geometries were studied, and we found a maximum jet velocity of 94 ± 3 m/s for a channel diameter of 120 μm, chamber length of 200 μm, and taper ratio of 0.25.

The dynamics of the liquid–air interface inside the microfluidic device determines the velocity and shape of the jet expelled. The meniscus focuses the liquid inside the channel leading to a fast and sharp curved shape jet. As the taper ratio is reduced, the jet velocity increases and the same for chamber depth. However, if the surface is nearest to the initial bubble and with a contact angle ≤ 74 deg, then the speed remains almost constant with the variation of the geometrical parameters. Penetration depths into agarose 1% gel up to 1 mm were reached.

In this work, the potential of CW-laser based microfluidic systems as needle-free drug injector has been demonstrated. The significant advantage of our proposition is that less energy to produce liquid microjets is required than with pulsed lasers, besides its lower cost and better portability. However, further studies of penetration depth into skin need to be carried out to fully validate this technique. In particular, higher volumes will be required to reap the benefits of CW-laser based jet injection.

Disclosures

The authors have no relevant financial interests in this article and no potential conflicts of interest to disclose.

Acknowledgments

The authors acknowledge financial support from CONACyT-Mexico and are grateful to Prof. Detlef Lohse and Prof. Chao Sun from POF for their support, advice, and access to their laboratory equipment. Also, a special thanks to Remco Sanders and Jeroen Korterik for laboratory assistance. DFR acknowledges the recognition from the Royal Dutch Society of Sciences (KHMW) that granted the Pieter Langerhuizen Lambertuszoon Fonds, 2016.

References

1. Y. Chartier et al., *Safe Management of Wastes from Health-Care Activities*, World Health Organization, Geneva (2014).
2. S. R. Reid, "Injection drug use, unsafe medical injections, and HIV in Africa: a systematic review," *Harm Reduct. J.* **6**, 24 (2009).
3. H. P. Kaphle et al., "Awareness and practices on injection safety among nurses working in hospitals of Pokhara, Nepal," *Int. J. Med. Health Sci.* **3**(4), 301–307 (2014).
4. B. G. Weniger and M. J. Papania, "Alternative vaccine delivery methods," in *Vaccines*, 5th ed., S. Plotkin, Ed., pp. 1357–1392, Elsevier, Amsterdam (2008).
5. N. C. Hogan et al., "Needle-free delivery of macromolecules through the skin using controllable jet injectors," *Expert Opin. Drug Delivery* **12**(10), 1637–1648 (2015).
6. J. Schramm-Baxter and S. Mitragotri, "Needle-free jet injections: dependence of jet penetration and dispersion in the skin on jet power," *J. Controlled Release* **97**, 527–535 (2004).
7. J. Schramm-Baxter, J. Katrencik, and S. Mitragotri, "Jet injection into polyacrylamide gels: investigation of jet injection mechanics," *J. Biomech.* **37**, 1181–1188 (2004).
8. A. C. Sintov et al., "Radiofrequency-driven skin microchanneling as a new way for electrically assisted transdermal delivery of hydrophilic drugs," *J. Controlled Release* **89**, 311–320 (2003).
9. J. C. Stachowiak et al., "Dynamic control of needle-free jet injection," *J. Controlled Release* **135**, 104–112 (2009).
10. A. Taberner, N. C. Hogan, and I. W. Hunter, "Needle-free jet injection using real-time controlled linear Lorentz-force actuators," *Med. Eng. Phys.* **34**, 1228–1235 (2012).
11. S. R. G. Avila, C. Song, and C.-D. Ohl, "Fast transient microjets induced by hemispherical cavitation bubbles," *J. Fluid Mech.* **767**, 31–51 (2015).
12. A. Arora et al., "Needle-free delivery of macromolecules across the skin by nanoliter-volume pulsed microjets," *Proc. Natl. Acad. Sci. U. S. A.* **104**, 4255–4260 (2007).
13. C. M. G. J. Houtzagers et al., "The Medi-Jector II: efficacy and acceptability in insulin-dependent diabetic patients with and without needle phobia," *Diabetic Med.* **5**, 135–138 (1988).
14. A. Arora, M. R. Prausnitz, and S. Mitragotri, "Micro-scale devices for transdermal drug delivery," *Int. J. Pharm.* **364**, 227–236 (2008).
15. M. Kendall, T. Mitchell, and P. Wrighton-Smith, "Intradermal ballistic delivery of micro-particles into excised human skin for pharmaceutical applications," *J. Biomech.* **37**, 1733–1741 (2004).
16. M. Kendall, "Engineering of needle-free physical methods to target epidermal cells for DNA vaccination," *Vaccine* **24**, 4651–4656 (2006).
17. Y. Tagawa et al., "Highly focused supersonic microjets," *Phys. Rev. X* **2**, 031002 (2012).
18. M. A. Park et al., "Er:YAG laser pulse for small-dose splashback-free microjet transdermal drug delivery," *Opt. Lett.* **37**, 3894 (2012).
19. H. J. Jang et al., "Laser-induced microjet: wavelength and pulse duration effects on bubble and jet generation for drug injection," *Appl. Phys. B* **113**, 417–421 (2013).
20. T. Han and J. J. Yoh, "A laser based reusable microjet injector for transdermal drug delivery," *J. Appl. Phys.* **107**, 103110 (2010).
21. H.-J. Jang et al., "Towards clinical use of a laser-induced microjet system aimed at reliable and safe drug delivery," *J. Biomed. Opt.* **19**, 058001 (2014).
22. E.-A. Brujan et al., "Dynamics of laser-induced cavitation bubbles near an elastic boundary," *J. Fluid Mech.* **433**, 251–281 (2001).
23. E.-A. Brujan et al., "Dynamics of laser-induced cavitation bubbles near elastic boundaries: influence of the elastic modulus," *J. Fluid Mech.* **433**, 283–314 (2001).
24. Y. Tagawa et al., "Needle-free injection into skin and soft matter with highly focused microjets," *Lab Chip* **13**, 1357–1363 (2013).
25. A. Philipp and W. Lauterborn, "Cavitation erosion by single laser-produced bubbles," *J. Fluid Mech.* **361**, 75–116 (1998).
26. W. D. Song, "Laser-induced cavitation bubbles for cleaning of solid surfaces," *J. Appl. Phys.* **95**(6), 2952–2956 (2004).
27. C. Berrospe-Rodriguez et al., "Continuous-wave laser generated jets for needle free applications," *Biomicrofluidics* **10**(1), 014104 (2016).
28. S. F. Rastopov and A. T. Sukhodolsky, "Sound generation by thermocavitation induced CW-laser in solutions," *Proc. SPIE* **1440**, 127–134 (1991).
29. J. C. Ramirez-San-Juan et al., "Time-resolved analysis of cavitation induced by CW lasers in absorbing liquids," *Opt. Express* **18**, 8735–8742 (2010).
30. J. P. Padilla-Martinez et al., "Optic cavitation with CW lasers: a review," *Phys. Fluids* **26**, 122007 (2014).
31. F. Li et al., "Oscillate boiling from microheaters," *Phys. Rev. Fluids* **2**, 014007 (2017).
32. J. Sandby-Moslalshller, T. Poulsen, and H. C. Wulf, "Epidermal thickness at different body sites: relationship to age, gender, pigmentation, blood content, skin kind and smoking habits," *Acta Derm. Venereol.* **83**(6), 410–413 (2003).
33. K. B. M. Q. Zaman, *Spreading Characteristics and Thrust of Jets from Asymmetric Nozzles*, National Aeronautics and Space Administration, Reno (1995).
34. P. A. Quinto-Su, K. Y. Lim, and C.-D. Ohl, "Cavitation bubble dynamics in microfluidic gaps of variable height," *Phys. Rev. E* **80**, 047301 (2009).
35. A. K. Dąbrowska et al., "Materials used to simulate physical properties of human skin," *Skin Res. Technol.* **22**(1), 3–14 (2016).
36. A. D. Maxwell et al., "A tissue phantom for visualization and measurement of ultrasound-induced cavitation damage," *Ultrasound Med. Biol.* **36**, 2132–2143 (2010).
37. P. G. Agache et al., "Mechanical properties and Young's modulus of human skin in vivo," *Arch. Dermatol. Res.* **269**, 221–232 (1980).
38. M. Ahearne et al., "Characterizing the viscoelastic properties of thin hydrogel-based constructs for tissue engineering applications," *J. R. Soc. Interface* **2**, 455–463 (2005).
39. J. M. Walker et al., "Nondestructive evaluation of hydrogel mechanical properties using ultrasound," *Ann. Biomed. Eng.* **39**(10), 2521–2530 (2011).
40. I. R. Peters et al., "Highly focused supersonic microjets: numerical simulations," *J. Fluid Mech.* **719**, 587–605 (2013).
41. E. Jens and V. Emmanuel, "Physics of liquid jets," *Rep. Prog. Phys.* **71**, 036601 (2008).
42. Y. A. Cengel and J. M. Cimbala, *Fluid Mechanics, Fundamentals and Applications*, McGraw Hill, New York (2006).
43. W. van Hoeve et al., "Breakup of diminutive Rayleigh jets," *Phys. Fluids* **22**(12), 122003 (2010).
44. V. Menezes, S. Kumar, and K. Takayama, "Shock wave driven liquid microjets for drug delivery," *J. Appl. Phys.* **106**, 086102 (2009).
45. H. Gelband et al., "The state of the world's antibiotics 2015," *Wound Healing South. Afr.* **8**(2), 30–34 (2015).
46. R. Krisiak et al., "Growth hormone therapy in children and adults," *Pharmacol. Rep.* **59**(5), 500–516 (2007).
47. R. Price et al., "Local injection treatment of tennis elbow—hydrocortisone, triamcinolone and lignocaine compared," *Rheumatology* **30**(1), 39–44 (1991).
48. S.-A. Sölveborn et al., "Cortisone injection with anesthetic additives for radial epicondylalgia (tennis elbow)," *Clin. Orthop. Relat. Res.* **316**, 99–105 (1995).
49. M. C. Riddle et al., "New insulin glargine 300 units/mL versus glargine 100 units/mL in people with type 2 diabetes using basal and mealtime insulin: glucose control and hypoglycemia in a 6-month randomized controlled trial (EDITION 1)," *Diabetes Care* **37**(10), 2755–2762 (2014).
50. Novo Nordisk, "How to start and convert your adult patients to once-daily, long-acting Tresiba," Tresiba, https://www.tresibapro.com/dosing-and-device/starting-patients.html (21 April 2017).
51. A. Aggarwal and A. Dutta, "Timing and dose of BCG vaccination in infants as assessed by postvaccination tuberculin sensitivity," *Indian Pediatr.* **32**(6), 635–639 (1995).
52. U.S. Department of Health & Human Service, "Seasonal influenza vaccine dosage and administration," Centers of Disease Control and Prevention, https://www.cdc.gov/flu/about/qa/vaxadmin.htm (21 April 2017).
53. M. G. Barnes, C. Ledford, and K. Hogan, "A needling problem: shoulder injury related to vaccine administration," *J. Am. Board Fam. Med.* **25**(6), 919–922 (2012).
54. S. H. Lee et al., "The current practice of skin testing for antibiotics in Korean hospitals," *Korean J. Intern. Med.* **25**(2), 207–212 (2010).
55. N. J. Chinoy et al., "Microdose vasal injection of sodium fluoride in the rat," *Reprod. Toxicol.* **5**(6), 505–512 (1991).

56. B. Kuhn and D. Wagner, "Package for delivering microdoses of medicament," U.S. Patent Application No. 13/816,455 (2011).
57. S. Vassileva and E. Hristakieva, "Medical applications of tattooing," *Clin. Dermatol.* **25**(4), 367–374 (2007).
58. C. A. Grant, P. C. Twigg, and D. J. Tobin, "Nano-scale observations of tattoo pigments in skin by atomic force microscopy," in *Tattooed Skin and Health*, J. Serup, N. Kluger, and W. Bäumler, Eds., Vol. **48**, pp. 97–102, Karger Publishers, Basel (2015).
59. International Medical Equipment, "MadaJet," MADA, http://www.madamedical.com/category/madajet/ (21 April 2017).
60. F. Pass and J. Hayes, *Needle-Free Drug Delivery*, Marcel Dekke, New York (2003).
61. InsuJet, "Insujet, for optimal insuline therapy," http://insujet.com/ (21 April 2017).
62. E. L. Giudice and J. D. Campbell, "Needle-free vaccine delivery," *Adv. Drug Delivery Rev.* **58**(1), 68–89 (2006).
63. J. L. Brandes et al., "Needle-free subcutaneous sumatriptan (Sumavel DosePro): bioequivalence and ease of use," *Headache: J. Head Face Pain* **49**(10), 1435–1444 (2009).
64. MIT Canada, "Med-jet," http://www.mitcanada.ca/ (21 April 2017).
65. S. S. Rao et al., "Comparative evaluation of three different intramuscular delivery methods for DNA immunization in a nonhuman primate animal model," *Vaccine* **24**, 367–373 (2006).
66. A. M. Römgens et al., "Penetration and delivery characteristics of repetitive microjet injection into the skin," *J. Controlled Release* **234**, 98–103 (2016).
67. M. D. Njoo et al., "Nonsurgical repigmentation therapies in vitiligo," *Arch. Dermatol.* **134**, 1–4 (1998).
68. Y. Sugiyama and S. Yamashita, "Impact of microdosing clinical study—why necessary and how useful?" *Adv. Drug Delivery Rev.* **63**(7), 494–502 (2011).
69. G. Lappin and R. C. Garner, "The utility of microdosing over the past 5 years," *Expert Opin. Drug Metab. Toxicol.* **4**, 1499–1506 (2008).
70. N. J. Chinoy et al., "Microdose vasal injection of sodium fluoride in the rat," *Reprod. Toxicol.* **5**(6), 505–512 (1991).
71. A. Kiyama et al., "Effects of a water hammer and cavitation on jet formation in a test tube," *J. Fluid Mech.* **787**, 224–236 (2016).
72. K. A. Holbrook and G. F. Odland, "Regional differences in the thickness (cell layers) of the human stratum corneum: an ultrastructural analysis," *J. Invest. Dermatol.* **62**, 415–422 (1974).

Biographies for the authors are not available.